

Dry Sliding Friction and Wear Properties of Al–25Zn–3Cu–(0–5)Si Alloys in the As-Cast and Heat-Treated Conditions

Temel Savaşkan · Osman Bican

Received: 31 August 2009 / Accepted: 12 July 2010 / Published online: 25 July 2010
© Springer Science+Business Media, LLC 2010

Abstract Dry sliding friction and wear properties of ternary Al–25Zn–3Cu and quaternary Al–25Zn–3Cu–(1–5)Si alloys were investigated using a pin-on-disc test machine after examining their microstructures and mechanical properties. An alloy (Al–25Zn–3Cu–3Si), which exhibited the highest tensile and compressive strengths, was subjected to T7 heat treatment. Surface and subsurface of the wear samples were investigated using scanning electron microscopy (SEM). The hardness and both tensile and compressive strengths of the alloys increased with increasing silicon content, but the trend reversed for the latter ones above 3% Si. It was observed that T7 heat treatment reduced the hardness and both tensile and compressive strengths of the Al–25Zn–3Cu–3Si alloy, but increased its elongation to fracture greatly. Three distinct regions were observed underneath the surface of the wear samples of the Al–25Zn–3Cu–3Si alloy. The formation of these regions was related to the heavy deformation of surface material and mixing, oxidation and smearing of wear material. Al–25Zn-based ternary and quaternary alloys in both as-cast and heat-treated conditions were found to be superior to SAE 660 bronze as far as their mechanical and dry sliding wear properties are concerned.

Keywords Unlubricated friction · Non-ferrous alloys · Wear mechanisms, SEM

1 Introduction

A number of zinc-based ternary and quaternary alloys such as ALZEN 305, ZA-5, ZA-8, ZA-12, ZA-27 and Zn–40Al–2Cu–2Si have been developed as a result of extensive research [1–6]. These alloys in general were found to be superior to the traditional bearing materials including bronze and cast iron as far as their wear resistance is concerned [7–12]. Amongst them the highest strength and wear resistance were obtained from the monotectoid Zn–40Al–2Cu, Zn–40Al–2Si and Zn–40Al–2Cu–2Si alloys [13–16]. However, the copper containing zinc-based ternary and quaternary alloys showed low ductility and considerable amount of dimensional instability [17–19]. Recently it has been shown that these problems can be overcome to a great extent by replacing zinc with aluminium [20–22]. Extensive research on the new alloys resulted in the development of ternary Al–40Zn–3Cu and Al–25Zn–3Cu and quaternary Al–40Zn–3Cu–2Si and Al–40Zn–3Cu–(1–3)Ni alloys [20–22]. They were found to be comparable to the zinc-based commercial alloys as far as their specific strength and wear resistance are concerned, but exhibited considerably higher ductility and lower dimensional change [1–12, 20–22]. However, the mechanical and tribological properties of Al–25Zn–3Cu-based quaternary alloys containing silicon have not been investigated. Therefore, the aim of this study was to investigate the dry sliding wear behaviour of Al–25Zn–3Cu–(1–5)Si alloys in a systematic manner after determining their structural and mechanical properties and compare the results with those of the SAE 660 bearing bronze under the same test conditions.

T. Savaşkan (✉) · O. Bican
Mechanical Engineering Department, Karadeniz Technical
University, Kanuni Campus, 61080 Trabzon, Turkey
e-mail: savaskan@ktu.edu.tr

2 Experimental Procedure

2.1 Preparation of Alloys and Examination of Microstructure

One ternary Al–25Zn–3Cu and six quaternary Al–25Zn–3Cu–(1–5)Si were prepared from commercially pure aluminium (99.7%), high purity zinc (99.9%), electrolytic copper (99.99%) and an Al–12Si eutectic alloy. Alloys were melted in an electric furnace and poured at a temperature of 680 °C into a steel mould at room temperature. The mould had a conical shape with a length of 180 mm, diameter of 57 mm at the bottom and diameter of 70 mm at the top. To compare the wear behaviour of Al–25Zn–3Cu-based alloys with that of a traditional bearing material, cylindrical ingot of centrifugally cast SAE 660 bronze (CuSn7ZnPb) was obtained from a commercial source.

The chemical compositions of the alloys were determined by atomic absorption analysis. Samples for structural examinations were prepared using standard metallographic techniques. The Al–25Zn–3Cu-based alloys were etched with 3% NaOH solution, and a solution consisting of 2 g FeCl₃ + 5 ml HCl + 30 ml H₂O + 60 ml ethanol was used for etching the bronze. Both alloys were examined using optical and scanning electron microscopy (SEM).

2.2 Physical and Mechanical Tests

The density of the alloys was determined by measuring their volume and mass. The Brinell hardness of the alloys was measured using a load of 62.5 kgf and a 2.5-mm steel ball as the indenter. The tensile and compressive strengths of the alloys were measured using round specimens with

the dimensions (diameter × gauge length) of 8 mm × 40 mm and 10 mm × 10 mm, respectively, at a strain rate of $5.9 \times 10^{-3} \text{ s}^{-1}$. Vicker's microhardness measurements were made on the samples after wear tests at a load of 10 gf. At least three readings were taken to determine the density, hardness, tensile and compressive strengths and elongation to fracture of the alloys.

2.3 Heat Treatment

Only the Al–25Zn–3Cu–3Si alloy, which exhibited the highest tensile and compressive strengths amongst the Al–25Zn-based alloys, was subjected to T7 heat treatment in order to improve its dimensional stability and ductility. The treatment was performed by solutionizing the alloy at a temperature of 375 °C for 36 h followed by rapid water quenching and ageing at 180 °C for 8 h. The ageing time for this heat treatment was determined using the hardness versus ageing time curve obtained at the same temperature for a total period of 100 h.

2.4 Friction and Wear Tests

The friction and wear tests were carried out using a pin-on-disc machine. A sectional view of this machine is shown in Fig. 1. The machine consists of a disc, a pin (specimen), a mounting system, a loading system, and friction force and temperature measurement system. The disc was made of SAE 1045 steel, the chemical composition of which is given in Table 1. The hardness of the disc was measured as 50 ± 1 HRC, after through hardening and tempering treatments.

Fig. 1 A schematic diagram of the pin-on-disc machine

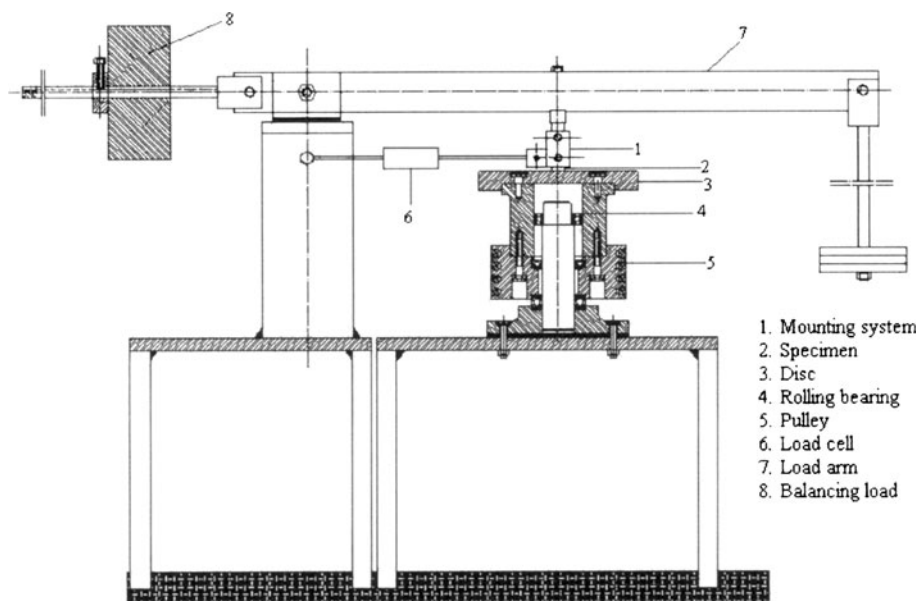


Table 1 Chemical composition of SAE 1045 steel

Material	Chemical composition (wt%)				
	C	Mn	P	S	Fe
SAE 1045	0.46	0.6	0.035	0.03	Balance

Wear samples with the dimensions of $10 \times 15 \times 25$ mm were prepared from the alloys including the SAE 660 bronze. Friction and wear tests were performed under a constant pressure of 1.5 MPa and a sliding speed of 1 m s^{-1} . The friction force was determined during sliding using a load cell (S-50), and the friction coefficient of the alloys was calculated by dividing friction force by the normal load. The friction and wear tests were carried out for 41.6 min, which corresponds to a sliding distance of 2,500 m. The temperature of the wear samples was monitored by inserting a copper–nickel thermocouple in a hole at a distance of 1.5 mm from the rubbing surface. The specimens were ultrasonically cleaned and weighed before each wear test using a balance with an accuracy of 0.01 mg. The disc was cleaned with organic solvents to remove surface contaminants before each test. The wear samples were removed after a sliding distance of 500 m, cleaned in solvents and weighed to determine the mass loss. This procedure was repeated for a total sliding distance of 2,500 m. The measured values of mass loss for all the specimens tested were converted into volume loss using the measured density of the alloys. The surface and sub-surface regions of the wear samples were examined using the secondary electron mode of SEM.

3 Results

3.1 Chemical Composition and Microstructure

The chemical compositions of ternary Al–25Zn–3Cu and quaternary Al–25Zn–3Cu–(1–5)Si alloys and the SAE 660 bronze are given in Tables 2 and 3, respectively.

The microstructures of the ternary Al–25Zn–3Cu alloy consisted of aluminium-rich α dendrites, eutectoid $\alpha+\eta$ and θ phases, Fig. 2a. The quaternary Al–25Zn–3Cu–(1–5)Si alloys revealed silicon particles in their microstructures, in addition to the phases observed in the ternary alloy, Fig. 2b–d. The size and distribution of the silicon particles were found to be dependent on the silicon content of the alloys. For example, they showed a fine appearance and a homogenous distribution in the alloys containing up to 3% Si. However, in the alloys containing more than 3% Si they became larger and exhibited an inhomogeneous distribution giving rise to a kind of micro-segregation by piling up in different locations. The dendritic microstructure of the

Table 2 Chemical composition of the alloys tested

Alloy	Chemical composition (wt%)			
	Al	Zn	Cu	Si
Al–25Zn–3Cu	71.7	25.2	3.1	–
Al–25Zn–3Cu–1Si	70.9	25.1	2.9	1.1
Al–25Zn–3Cu–2Si	69.8	25.2	2.8	2.2
Al–25Zn–3Cu–2.5Si	69.4	25.1	2.9	2.6
Al–25Zn–3Cu–3Si	68.9	25.1	2.9	3.1
Al–25Zn–3Cu–4Si	67.8	25.2	3.1	3.9
Al–25Zn–3Cu–5Si	67.0	25.1	2.8	5.1

Table 3 Chemical composition of the SAE 660 bronze

Alloy	Chemical composition (wt%)			
	Cu	Sn	Pb	Zn
SAE 660 bronze	82.8	6.9	5.7	4.6

Al–25Zn–3Cu–3Si alloy was completely removed after T7 heat treatment as seen in Fig. 2e. The microstructure of the SAE 660 bronze consisted of copper-rich α , eutectoid $\alpha + \delta$ and lead-rich phases, Fig. 2f.

3.2 Physical and Mechanical Properties

The variation of hardness, tensile and compressive strength, density and percentage elongation to fracture of Al–25Zn–3Cu–(0–5) alloys as a function of silicon content are shown in Fig. 3.

It can be seen that the tensile and compressive strengths of the alloys showed three distinct changes with silicon content. These include an initial sharp decrease with increasing Si content, a gradual increase between 1 and 3% Si and a sharp decrease once again at still higher contents. However, their hardness increased continuously with increasing silicon content, whilst density and percentage elongation to fracture decreased.

The curve showing the change in hardness of the supersaturated Al–25Zn–3Cu–3Si alloy with ageing time at a temperature of 180 °C is given in Fig. 4. This curve was used to determine the duration of T7 heat treatment. The hardness of the alloy initially increased with increasing ageing time, but showed a sharp decrease after reaching its highest value. The values of hardness, tensile and compressive strengths and elongation to fracture of the alloy subjected to T7 heat treatment are given in Table 4. It can be seen that the T7 heat treatment applied to the alloy reduced its hardness and both tensile and compressive strengths, but increased elongation to fracture.

Fig. 2 Microstructures of **a** Al–25Zn–3Cu, **b** Al–25Zn–3Cu–1Si, **c** Al–25Zn–3Cu–3Si, **d** Al–25Zn–3Cu–5Si (heat-treated) and **f** SAE 660 bronze alloys

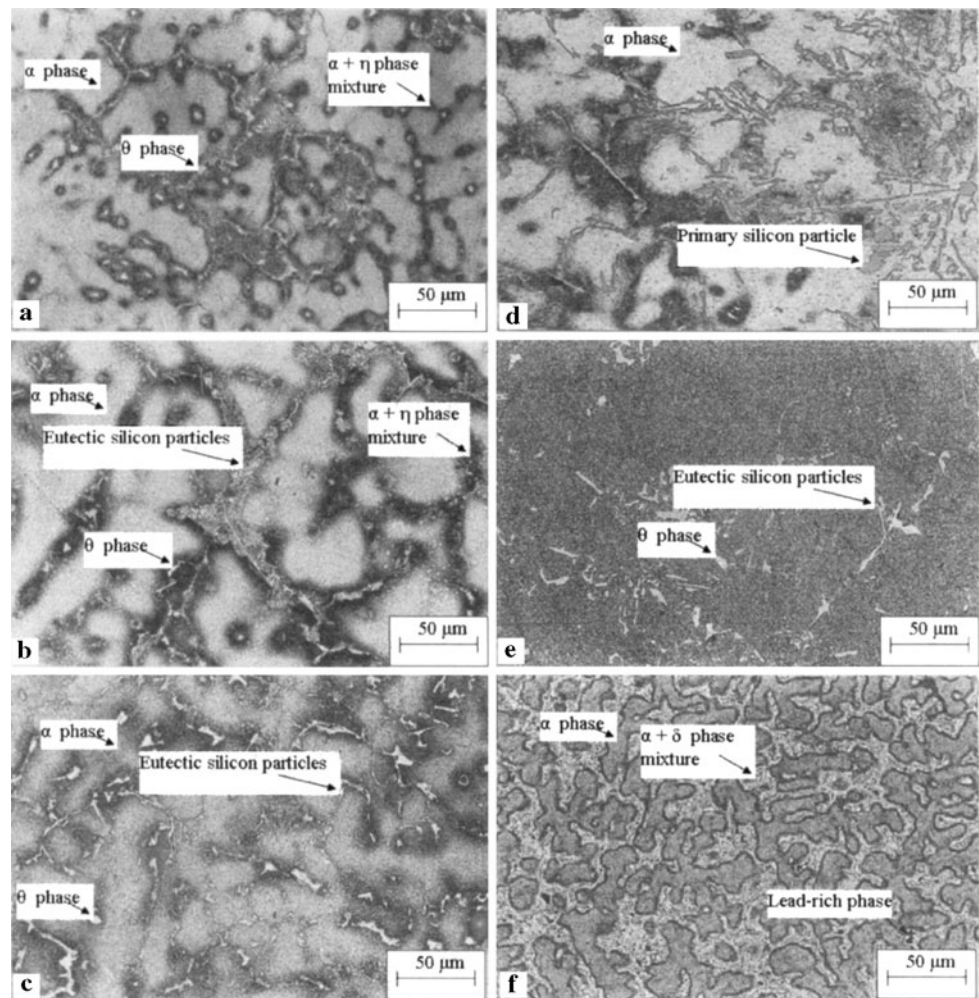
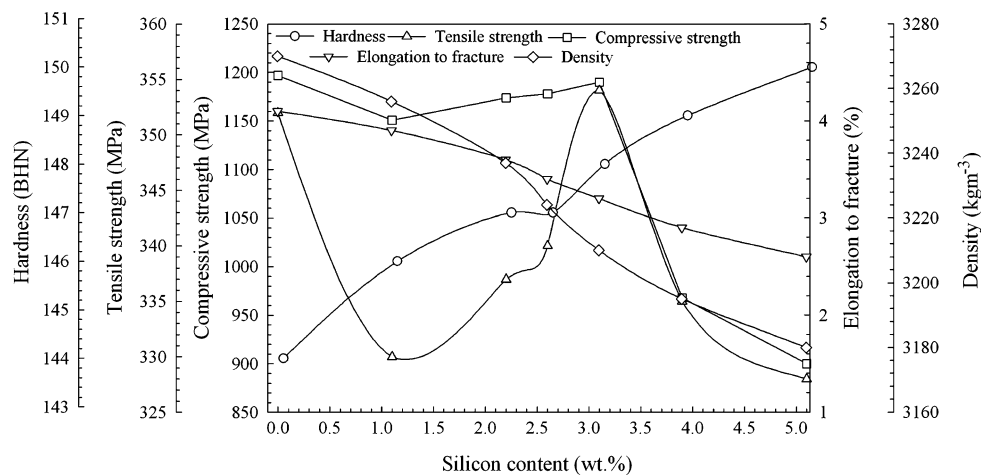


Fig. 3 The change in density, hardness, tensile and compressive strengths and percentage elongation to fracture of the alloys with silicon content



3.3 Friction and Wear Test Results

The friction coefficient and temperature versus sliding distance curves for the alloys are shown in Figs. 5 and 6, respectively. The friction coefficient and temperature of the alloys showed a sharp increase during the initial period of

test run and reached almost constant levels after approximately 200 m sliding distance. However, the constant values of the friction coefficient and temperature of the Al–25Zn–3Cu–(0–5)Si alloys were found to be considerably lower than those of the SAE 660 bronze. The lowest friction coefficient and temperature values were obtained

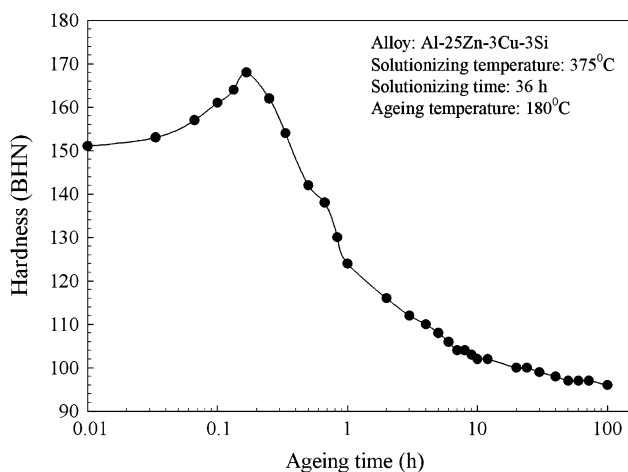


Fig. 4 Hardness versus ageing time curve for the Al-25Zn-3Cu-3Si alloy

from the Al-25Zn-3Cu alloy, whilst the SAE 660 bronze showed the highest values of these parameters.

The wear volume versus sliding distance curves for the alloys tested are given in Fig. 7. The wear volume of the alloys increased almost linearly with sliding distance. The lowest wear volume was obtained from the Al-25Zn-3Cu-3Si alloy, whilst the SAE 660 bronze exhibited the highest wear volume.

The curves showing the change of friction coefficient, temperature and wear volume as a function of silicon content of the quaternary alloys are given in Fig. 8. It can be seen that the steady state values of the friction coefficient and temperature of the alloys increased continuously with increasing silicon content. However, the wear volume of the alloys increased with increasing silicon content up to 3%, above which the trend reversed.

The wear surfaces of the ternary Al-25Zn-3Cu and quaternary Al-25Zn-3Cu-3Si alloys were characterized by smearing and scratches, but the smearing/adhesion was found to be the dominant mechanism, as seen in Fig. 9a and b. However, the wear surface of the SAE 660 bronze was almost covered by continuous scratches and showed a little amount of smearing with a few microcracks, Fig. 9c.

Three different regions were observed underneath the surface of the wear samples of the Al-25Zn-3Cu-3Si alloy tested for a sliding distance of 2,500 m. A micrograph

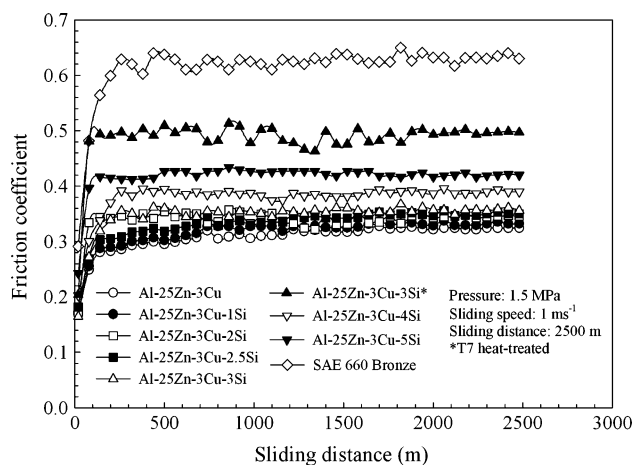


Fig. 5 Friction coefficient versus sliding distance curves for the alloys tested

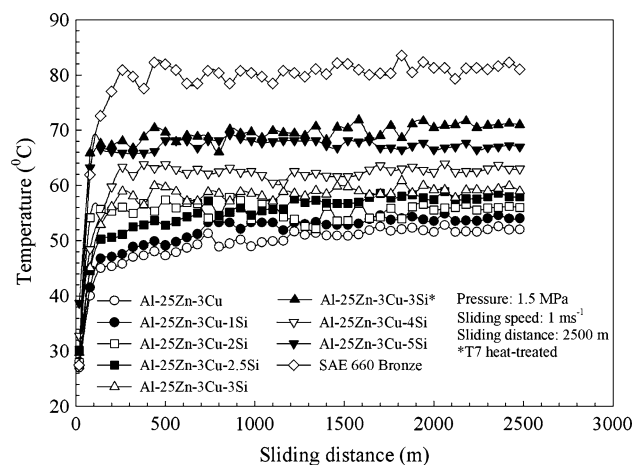


Fig. 6 The variation of temperature of the alloys tested as a function of sliding distance

showing these regions labelled as A, B and C and corresponding microhardness profile is given in Fig. 10. It can be seen that the region A, which appears to be a surface layer, has a very fine microstructure and the region B shows the flow lines oriented in the sliding direction. It is interesting to note that the silicon particles, which were observed to be long and large in the original microstructure, appear as fine ones in the region A. It can also be seen

Table 4 Mechanical properties of the Al-25Zn-3Cu-3Si alloy in the as-cast and heat-treated conditions and SAE 660 bronze

Alloy	Hardness (BHN)	Tensile strength (MPa)	Compressive strength (MPa)	Elongation to fracture (%)	Density (kg m ⁻³)
Al-25Zn-3Cu-3Si (as-cast)	148	354	1190	3.2	3210
Al-25Zn-3Cu-3Si (heat-treated)	104	298	1162	8.1	3212
SAE 660 bronze	83	278	1098	11.0	8913

Note: heat treatment was performed by quench-ageing of the alloy at a temperature of 180 °C for duration of 8 h

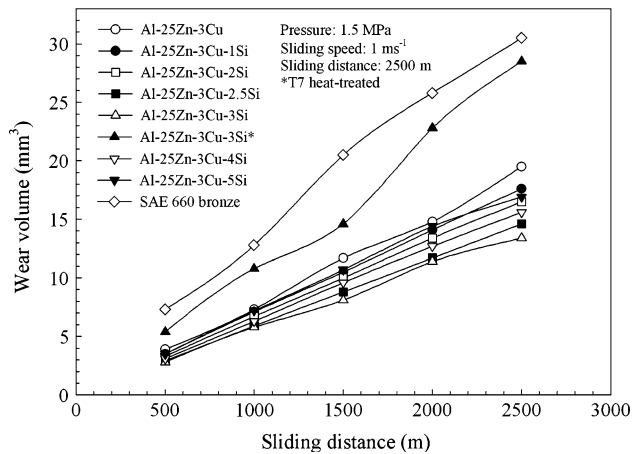


Fig. 7 Wear volume versus sliding distance plots for the alloys tested

that the microhardness of the wear sample decreases sharply with increasing depth from the surface, and shows a sharp increase after dropping to its lowest value and finally reaches the microhardness level of the original microstructure. This indicates that the region A has the highest where the region B exhibits the lowest microhardness. However, only limited flow lines oriented in the sliding direction were observed just below the surface of the wear samples of the SAE 660 bronze, Fig. 11.

4 Discussion

The microstructure of the ternary Al–25Zn–3Cu alloy consisted of aluminium-rich α dendrites, eutectoid $\alpha + \eta$ phase mixture and copper-rich θ phase, Fig. 2a. In addition to these phases, silicon particles were observed in the quaternary Al–25Zn–3Cu–(1–5)Si alloys, Fig. 2b–d. The silicon particles showed a fine appearance and homogeneous distribution in the quaternary alloys containing up to

3% Si. However, when the silicon content exceeded this level, some of the silicon particles became larger and gave rise to micro-segregation. Fine silicon particles are produced by eutectic transformation, and the large ones represent the primary silicon phase formed during solidification [4, 6, 9, 16, 20].

Hardness of the quaternary Al–25Zn–3Cu–(1–5)Si alloys increased with increasing silicon content, Fig. 3. Continuous increase in the hardness of the alloys with increasing silicon content can be related to the percentage amount of relatively hard and brittle silicon particles in their microstructures [6, 7, 16, 20]. The tensile and compressive strengths of the alloys showed three distinct regions including an initial decrease, a gradual increase between 1 and 3% Si and a final decrease as shown in Fig. 3. Changes in both tensile and compressive strengths of the alloys may be explained in terms of content, size, shape and distribution of the hard silicon particles. All the silicon particles in the alloy containing 1% Si appeared only in their interdendritic regions. Since these particles are relatively hard and brittle, they may give rise to cracking in the interdendritic regions under tension [6, 16, 20]. However, such brittleness has less adverse effect on the fracture behaviour of the alloys under compression. Therefore, the influence of silicon particles on the compressive strength is expected to be less effective than that observed in the case of the tensile strength. The silicon particles in the alloys containing 1–3% Si showed more homogeneous distribution and resulted in a gradual increase in both tensile and compressive strengths of the alloys, Fig. 3. However, both fine and large silicon particles were observed in the alloys containing more than 3% Si, Fig. 2c. In addition, they appeared to be elongated and showed a tendency to pile up in different locations. It appears that the size and the degree of segregation of silicon particles increase considerably when the silicon content exceeds 3%. It is known that the

Fig. 8 The change of the friction coefficient, temperature and wear volume of the alloys as a function of silicon content

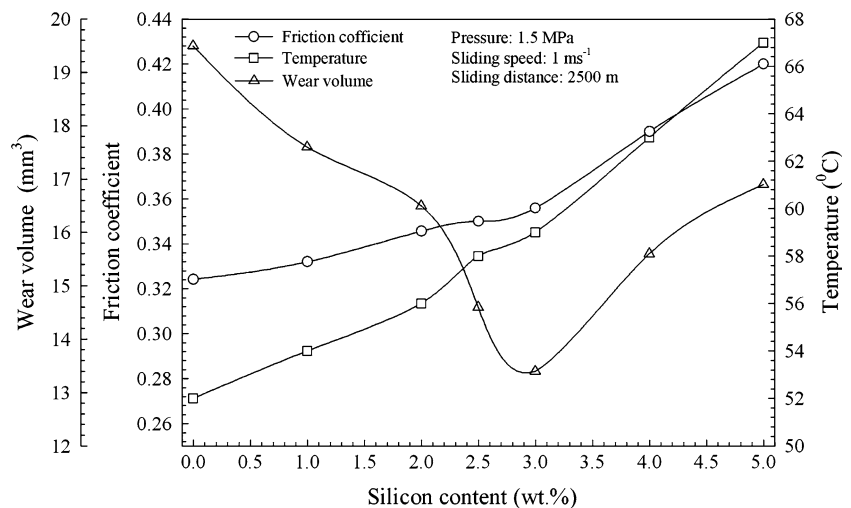


Fig. 9 Wear surfaces of **a** Al-25Zn-3Cu alloy, **b** Al-25Zn-3Cu-3Si alloy and **c** SAE 660 bronze tested at a pressure of 1.5 MPa and a sliding speed of 1 m s^{-1} for a total sliding distance of 2,500 m

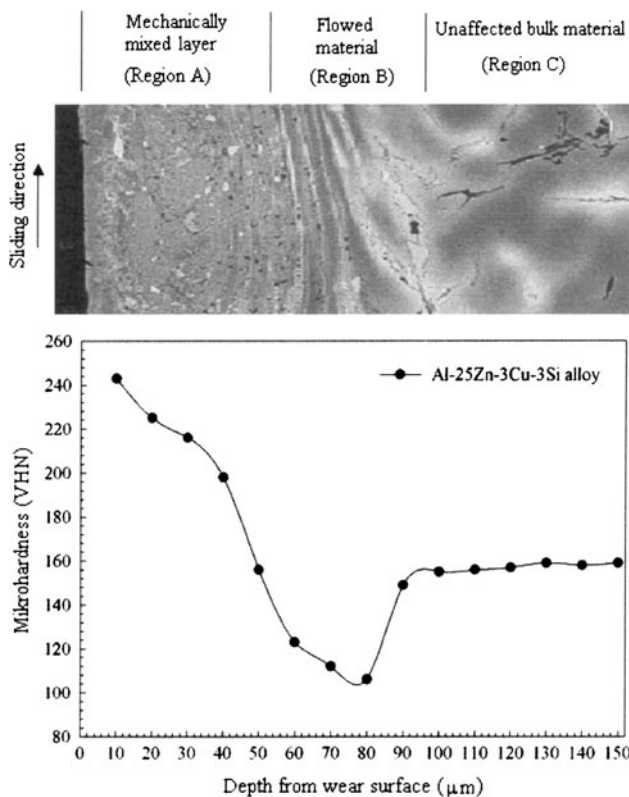
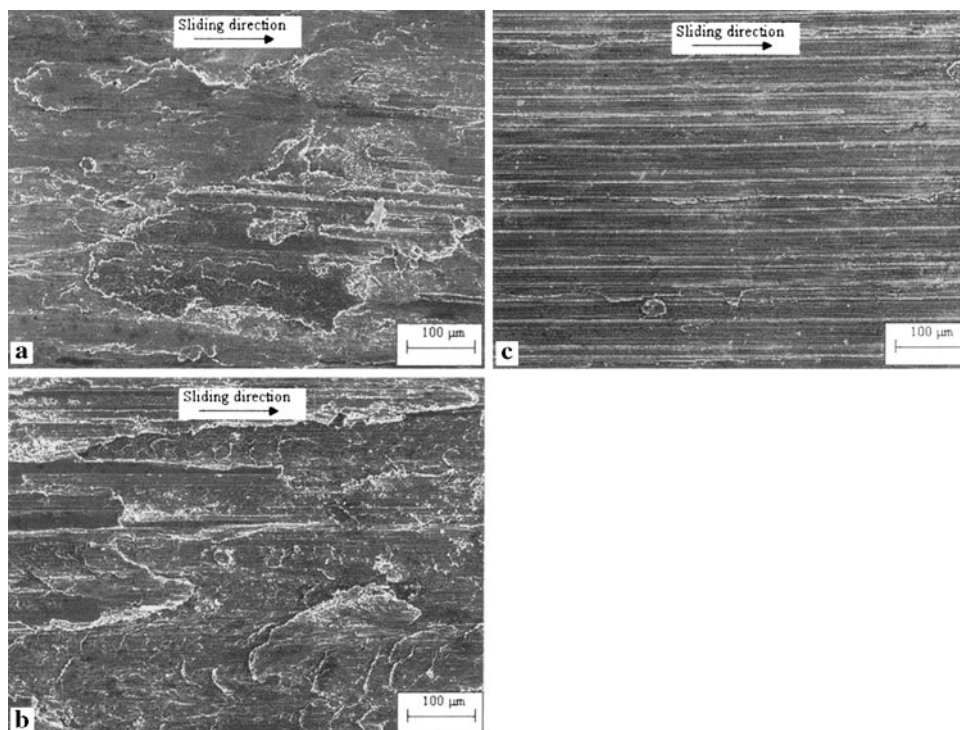


Fig. 10 Microstructural changes underneath the wear surface of the Al-25Zn-3Cu-3Si alloy and corresponding microhardness profile

formation of large primary silicon particles in either zinc or aluminium-based alloys results in a reduction in their strength by giving rise to cracking tendency [6, 16, 20].

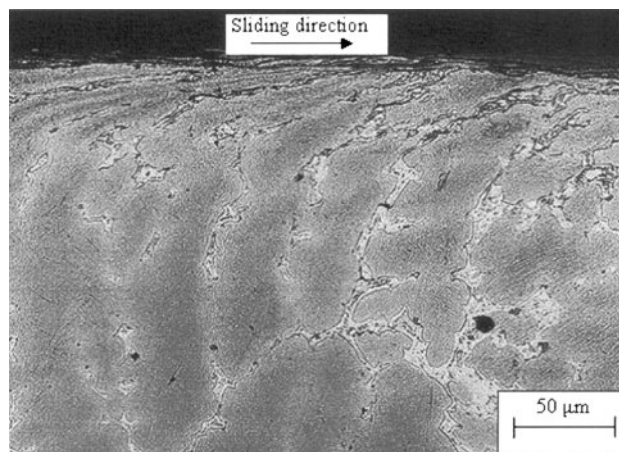


Fig. 11 Appearance of the microstructural changes underneath the wear surface of the SAE 660 bronze

This brittleness due to large and elongated silicon particles may also reduce the compressive strength of the alloys. Therefore, a reduction would be expected in both tensile and compressive strengths of the alloys when their silicon content exceeds 3%.

It was observed that the T7 heat treatment reduced the hardness and both tensile and compressive strengths of the Al-25Zn-3Cu-3Si alloy, but increased its percentage elongation considerably, Table 4. This can be explained in terms of the decomposition of the supersaturated solid solutions. The hardness of the alloy is expected to increase during ageing due to precipitation of zinc-rich phases.

However, it would be expected to decrease beyond the peak due to the coarsening of microconstituents, Fig. 4. An ageing time of 8 h at 180 °C was considered to be sufficient to obtain a stable microstructure by completing the major phase changes in the alloy [12, 13, 23–26].

The friction coefficient and temperature of the alloys showed a sharp increase during the initial period of the test and reached almost constant levels after a sliding distance of approximately 200 m, Figs. 5 and 6. These observations may be related to the smoothening out of the wear surfaces due to the wear-in process and formation of oxide films thereon [10, 27–29].

The wear volume of the alloys increased almost linearly with sliding distance, Fig. 7. The Al–25Zn–3Cu–3Si alloy possessing the highest tensile and compressive strengths showed the highest wear resistance amongst all. This is in agreement with the laws of adhesive wear and Archard's equation [30]. Wear volume of the alloys can also be related to their tensile and compressive strengths [11, 20–22]. It is known that as the tensile and compressive strengths of the alloys increase, their wear volume decreases [8, 11, 20–22]. In view of above, the Al–25Zn–3Cu–3Si alloy would be expected to exhibit the lowest wear volume. However, the wear resistance of this alloy decreased after heat treatment (T7). This observation can be related to the microstructural changes and deterioration in the hardness and strength of the alloy. The microstructural changes may be responsible for the change observed in wear behaviour of the alloy by producing a fine-grained matrix which gave rise to less smearing, whilst the deterioration in hardness and strength lowered its wear resistance.

Friction coefficient and temperature of the Al–25Zn–3Cu–(0–5)Si alloys increased continuously with increasing silicon content. However, the wear volume of the alloys decreased with increasing silicon content up to 3%, above which the trend reversed. It can be explained in terms of microstructural features and mechanical properties of these alloys. As mentioned above, addition of silicon forms eutectic and primary silicon particles in the microstructure. Since these particles are hard and brittle, they may increase the friction coefficient and temperature. On the other hand, the mechanical properties of these alloys are very sensitive to the size and distribution of the silicon particles. It is known that the primary silicon particles deteriorate the strength of the alloys [6, 20]. These particles were only observed in the Al–25Zn-based alloys containing more than 3% Si. Therefore, an increase would be expected in the wear volume of the alloys containing more silicon than this level.

Wear surfaces of the Al–25Zn–3Cu–Si alloys were characterized by smearing and scratches, Fig. 9a–b. However, only very limited amount of smearing together with fine and continuous scratches were observed on the wear surface of the SAE 660 bronze, Fig. 9c. Smearing may

have resulted from the back transfer of the wear material from disc to sample surface, whilst the scratches are produced by ploughing action of the hard wear particles during either their removal or back transferring [1, 3, 6, 9, 11, 15, 20, 31]. Three different regions were observed underneath the wear surface of Al–25Zn–3Cu–3Si alloy and they are called regions A, B and C, Fig. 10. The region A which appeared to be a continuous surface layer had a very fine microstructure, whilst the region B exhibited flow lines oriented to the sliding direction. However, the region C has the same microstructure as the unaffected bulk material. The microhardness profile obtained from the subsurface of the wear sample of this alloy showed that region A has the highest, but the region B has the lowest microhardness values, Fig. 10. These observations indicate that the region A was produced by grinding, mixing and smearing of the wear material due to combined effects of compressive and localized shear stresses on the wear surface. Therefore, it may be considered as a mechanically mixed surface layer. The flow lines observed in region B resulted from the severe plastic deformation of the surface material of the wear sample due to the shear stresses acting along the sliding direction and frictional heat. Similar explanations were reported in previous articles [22, 31–36]. As a result it may be suggested that the flow lines form first in the surface material of the wear sample then the region A builds up gradually by back transferring, mixing and smearing of the wear particles. This results in the formation of a fine grained layer with high hardness on the wear surface. However, the microhardness of region B was much lower than that of the unaffected bulk. This may be related to recrystallization which takes place in this region due to severe plastic deformation and frictional heat [37]. Surface and subsurface examinations suggest that adhesion including back transfer, mixing and smearing is the most effective wear mechanism for the Al–25Zn–3Cu–Si alloys, whilst the abrasion due to ploughing action of fine and hard wear particles dominates the wear of the SAE 660 bronze.

Compared to the SAE 660 bronze, the Al–25Zn–3Cu–(0–5)Si alloys exhibited lower friction coefficient and higher wear resistance under the same test conditions, Figs. 5, 6 and 7. This may be related to their microstructure and mechanical properties. These alloys have a multiphase structure consisting of aluminium-rich α , zinc-rich η and copper-rich θ phases and silicon particles [1, 3, 10, 15, 22, 27]. The α and η phases in the alloy microstructure are soft compared to the θ and silicon particles. This makes it an ideal microstructure for the bearing applications [5, 10, 15, 20–22, 27]. In addition, oxide films formed on the wear surfaces of these alloys during dry sliding lower their friction coefficient and improve their wear resistance [10, 15, 27]. This is because the aluminium oxide which is a hard compound provides load-carrying capability, whilst

the relatively soft zinc oxide acts as a lubricant [8, 10, 15, 27]. The hardness, tensile and compressive strengths of these alloys were found to be much higher than those of the SAE 660 bronze. Since the wear rate of most materials is inversely proportional to their hardness or strength, the Al–25Zn–3Cu–(0–5)Si alloys can be expected to have higher wear resistance than that of the SAE 660 bronze as far as the present test conditions are concerned. In addition, crack sensitivity of the bronze may also be responsible to a certain extent for its inferior wear response [10, 38].

5 Conclusions

- (1) The microstructure of the quaternary Al–25Zn–3Cu–(1–5)Si alloys consisted of aluminium-rich α , eutectoid $\alpha + \eta$ and copper-rich θ phases and eutectic and/or primary silicon particles.
- (2) The hardness and both tensile and compressive strengths of the Al–25Zn–3Cu-based alloys increased with increasing silicon content, but the trend reversed for the ones with more than 3% Si. Amongst the as-cast alloys, the highest wear resistance was obtained with the Al–25Zn–3Cu–3Si alloy.
- (3) The T7 heat treatment reduced the tensile and compressive strengths and wear resistance of the Al–25Zn–3Cu–3Si alloy, but greatly increased its ductility. Despite the decrease in the strengths of this alloy, its wear resistance in the heat-treated condition was found to be considerably higher than that of the bearing bronze. In addition, the wear resistance of the alloys tested was observed to be strongly dependent on their tensile and compressive strengths rather than their hardness as far as this study is concerned.
- (4) A fine-grained surface layer and a deformed region containing flow lines oriented in the sliding direction were observed underneath the wear surface of the Al–25Zn–3Cu–3Si alloy. Occurrence of the flow lines was related to the deformation and recrystallization of the surface material, and formation of the fine-grained surface layer was explained in terms of back transferring, mixing and smearing of the wear particles.

Acknowledgments The authors acknowledge the financial support provided by the Scientific and Technological Research Council of Turkey (TUBITAK). Grant no. 108M292.

References

1. Murphy, S., Savaşkan, T.: Comparative wear behaviour of Zn–Al based alloys in an automotive engine application. *Wear* **98**, 151–161 (1984)
2. Savaşkan, T., Murphy, S.: Mechanical properties and lubricated wear of Zn–25Al-based alloys. *Wear* **116**, 211–224 (1987)
3. Savaşkan, T., Turhal, M.Ş., Murphy, S.: Effect of cooling rate on the structure and mechanical properties of monotectoid zinc–aluminium alloys. *Mater. Sci. Technol. Lond.* **19**, 67–74 (2003)
4. Savaşkan, T., Murphy, S.: Creep behaviour of Zn–Al–Cu alloys. *Z. Metallkd.* **74**, 76–82 (1983)
5. Azakli, Z., Savaşkan, T.: An examination of frictional and sliding wear properties of Zn–40Al–2Cu–2Si alloy in case of oil cut off. *Tribol. Int.* **41**, 9–16 (2008)
6. Savaşkan, T., Bican, O.: Effects of silicon content on the microstructural features and mechanical and sliding wear properties of Zn–40Al–2Cu–(0–5)Si alloys. *Mater. Sci. Eng. A Struct.* **404**, 259–269 (2005)
7. Lee, P., Savaşkan, T., Laufer, E.: Wear resistance and microstructure of Zn–Al–Si and Zn–Al–Cu alloys. *Wear* **117**, 79–89 (1987)
8. Savaşkan, T., Pürçek, G., Hekimoğlu, A.P.: Effect of copper content on the mechanical and tribological properties of ZnAl27-based alloys. *Tribol. Lett.* **15**, 257–263 (2003)
9. Prasad, B.K.: Sliding wear response of a zinc-based alloy and its composite and comparison with a gray cast iron: influence of external lubrication and microstructural features. *Mater. Sci. Eng. A Struct.* **392**, 427–439 (2005)
10. Prasad, B.K., Patwardhan, A.K., Yegneswaran, A.H.: Dry sliding wear characteristics of some zinc–aluminium alloys: a comparative study with a conventional bearing bronze at a slow speed. *Wear* **199**, 142–151 (1996)
11. Savaşkan, T., Hekimoğlu, A.P., Pürçek, G.: Effect of copper content on the mechanical and sliding wear properties of monotectoid-based zinc–aluminium–copper alloys. *Tribol. Int.* **37**, 45–50 (2004)
12. Prasad, B.K.: Influence of heat treatment on the physical, mechanical and tribological properties of a zinc-based alloy. *Z. Metallkd.* **87**, 226–232 (1996)
13. Savaşkan, T., Azakli, Z.: An investigation of lubricated friction and wear properties of Zn–40Al–2Cu–2Si alloy in comparison with SAE 65 bearing bronze. *Wear* **264**, 920–928 (2008)
14. Prasad, B.K., Patwardhan, A.K., Yegneswaran, A.H.: Dry sliding wear response of a modified zinc-based alloy. *Mater. Trans. JIM* **38**, 197–204 (1997)
15. Pürçek, G., Savaşkan, T., Küçükömeroğlu, T., Murphy, S.: Dry sliding friction and wear properties of zinc-based alloys. *Wear* **252**, 894–901 (2002)
16. Prasad, B.K.: Effect of silicon addition and test parameters on the sliding wear characteristics of zinc-based alloy containing 37.5% aluminium. *Mater. Trans. JIM* **38**, 701–706 (1997)
17. Murphy, S.: Solid-state reactions in the low-copper part of the Al–Cu–Zn system. *Z. Metallkd.* **71**, 96–102 (1980)
18. Yaohua, Z., Murphy, S.: A general rule of decomposition reaction in supersaturated Zn–Al based alloys. *Chin. J. Mater. Sci. Technol.* **2**, 105–116 (1986)
19. Yaohua, Z.: Phase equilibria in Zn–Al–Cu–Si. *Chin. J. Mater. Sci. Technol.* **5**, 113–118 (1989)
20. Alemdağ, Y., Savaşkan, T.: Effects of silicon content on the mechanical properties and lubricated wear behaviour of Al–40Zn–3Cu–(0–5)Si alloys. *Tribol. Lett.* **29**, 221–227 (2008)
21. Alemdağ, Y., Savaşkan, T.: Mechanical and tribological properties of Al–40Zn–Cu alloys. *Tribol. Int.* **42**, 176–182 (2008)
22. Savaşkan, T., Bican, O., Alemdağ, Y.: Developing aluminium–zinc-based a new alloy for tribological applications. *J. Mater. Sci.* **44**, 1969–1976 (2009)
23. Oppenheim, T., Tewfic, S., Scheck, T., Klee, V., Lomeli, S., Dahir, W., Youngren, P., Aizpuru, N., Clark, R., Lee, E.W., Ogren, J., Es-Said, O.S.: On the correlation of mechanical and physical properties of 6061-T7 and 7249-T76 aluminum alloys. *Eng. Fail. Anal.* **14**, 218–225 (2007)
24. Akhter, R., Ivanchev, L., Burger, H.P.: Effect of pre/post T7 heat treatment on the mechanical properties of laser welded SSM cast

- A356 aluminium alloy. *Mater. Sci. Eng. A Struct.* **447**, 192–196 (2007)
25. Wang, Z., Li, Z., Ning, J., Zhao, L.: Effect of heat treatments on the crushing behaviour and energy absorbing performance of aluminium alloy foams. *Mater. Des.* **30**, 977–982 (2009)
 26. Guo, J., Yuan, X.: The aging behaviour of SiC/Gr/6013Al composite in T4 and T7 treatments. *Mater. Sci. Eng. A Struct.* **499**, 212–214 (2009)
 27. An, J., Liu, Y.B., Lu, Y.: The influence of Pb on the friction and wear behaviour of Al–Si–Pb alloys. *Mater. Sci. Eng. A Struct.* **373**, 294–302 (2004)
 28. Şahin, Y., Murphy, S.: The effect of sliding speed and microstructure on the dry wear properties of metal-matrix composites. *Wear* **214**, 98–106 (1998)
 29. Rodriguez, J., Poza, P., Garrido, M.A., Rico, A.: Dry sliding wear behaviour of aluminium–lithium alloys reinforced with SiC particles. *Wear* **262**, 292–300 (2007)
 30. Halling, J.: *Principles of Tribology*. Macmillan, Great Britain (1975)
 31. Prasad, B.K.: Investigation into sliding wear performance of zinc-based alloy reinforced with SiC particles in dry and lubricated conditions. *Wear* **262**, 262–273 (2007)
 32. Rice, S.L., Nowotny, H., Wayne, S.F.: Characteristics of metallic subsurface zones in sliding and impact wear. *Wear* **74**, 131–142 (1982)
 33. Pandey, J.P., Prasad, B.K.: Dry sliding wear behaviour of a zinc-based alloy against different counterface materials. *Z. Metallkd.* **88**, 739–743 (1997)
 34. Akarca, S.S., Altenhof, W.J., Alpas, A.T.: Subsurface deformation and damage accumulation in aluminium–silicon alloys subjected to sliding contact. *Tribol. Int.* **40**, 735–747 (2007)
 35. Rice, S.L., Nowotny, H., Wayne, S.F.: A survey of the development of subsurface zones in the wear of materials. *Key Eng. Mater.* **33**, 77–100 (1989)
 36. Prasada Rao, A.K., Das, K., Murty, B.S., Chakraborty, M.: Microstructure and wear mechanisms of grain-refined aluminium during dry sliding against steel disc. *Wear* **264**, 638–647 (2008)
 37. Savaşkan, T., Bican, O.: Dry sliding friction and wear properties of Al–25Zn–3Cu–3Si alloy. *Tribol. Int.* **43**, 1346–1352 (2010)
 38. Prasad, B.K., Patwardhan, A.K., Yegneswaran, A.H.: Factors controlling dry sliding wear behaviour of a leaded tin bronze. *Mater. Sci. Technol. Lond.* **12**, 427–435 (1996)